High Throughput Experimental and Theoretical Predictive Screening of Materials − A Comparative Study of Search Strategies for New Fuel Cell Anode Catalysts

Peter Strasser,* Qun Fan, Martin Devenney, and W. Henry Weinberg

Symyx Technologies, Inc., 3100 Central Expressway, Santa Clara, California 95051

Ping Liu and Jens K. Nørskov

Center for Atomic-scale Materials Physics, Department of Physics, Technical University of Denmark, Building 307, DK-2800 Lyngby, Denmark

Received: April 24, 2003

A comparative study of experimental and theoretical combinatorial and high-throughput screening methods for the development of novel materials is presented. Both methods were applied to the development of new anode fuel cell alloy catalysts with improved CO tolerance. Combinatorial experimental electrocatalysis was performed on a 64-element electrode array. Sputter-deposited ternary thin-film electrocatalysts of composition PtRuM (M = Co,Ni,W) were screened in parallel for their methanol oxidation activity, and their individual geometric and specific chronoamperometric current density were monitored and evaluated against standard PtRu catalysts. Density functional theory calculations of a variety of model ternary PtRuM alloy catalysts yielded detailed adsorption energies and activation barriers. Feeding these thermodynamic and kinetic data into a simple micro kinetic model for the CO electro oxidation reaction, the relative activities of a number of PtRuM ternary alloys were calculated. The experimental and theoretical computational results reveal very similar trends in electrocatalytic activity as a function of alloy composition; they also point at similar ternary PtRuM alloys as candidates for improved anode catalysts for low-temperature fuel cells.

1. Introduction

The polymer electrolyte membrane fuel cell (PEMFC) technology is currently considered as one of the most promising alternative energy conversion devices of the next decade for stationary, portable, and automotive applications. Complications in terms of cell efficiency and power density are minimized if a PEMFC is operated using pure hydrogen fuel on the anode and oxygen/air on the cathode. However, in the short term, this is unlikely to happen in a fuel-cell mass market due to numerous challenges associated with a hydrogen infrastructure. What appears more likely is a PEMFC operation mode using a liquid hydrocarbon fuel and a fuel processor where the fuel is first reformed into a hydrogen-rich, but CO-containing, gas, followed by the anodic electrooxidation of the hydrogen at the PEMFC anode catalyst. Alternatively and preferably for low-power applications, a PEMFC can be operated using a oxygenated small hydrocarbon fuel such as methanol that is fed directly into the PEMFC anode and becomes electrooxidized at the anode fuel cell catalyst (e.g., the direct methanol fuel cell, DMFC). For both H_2/CO gas and alcohol anode feeds, the observed power densities are much lower compared to the operation using pure hydrogen. In both cases, this is primarily due to a rapid deactivation and poisoning of the anode catalyst surface by CO, originating either from the H_2/CO gas phase, or in case of a DMFC, from CO that forms through the dissociative adsorption and subsequent H-stripping of methanol.[1,2]

Initially, pure Pt was used as the anode fuel cell catalyst. While it remained unclear how to suppress the adsorption and formation of surface-bound CO, remedies allowing the reduction of surface CO were found in the alloying of Pt with Ru and other metals such as Sn.[1,2] This resulted in significant increases of the CO tolerance of the Pt-alloy anode catalysts. To date, Pt−Ru alloys are still commonly accepted as the best and most stable anode electrocatalyst for both the oxidation of H_2/CO in PEMFCs and the oxidation of methanol in DMFCs. Despite progress through binary Pt−Ru alloys, the blocking of the anode catalyst surface by adsorbed CO still represents a serious material challenge of today's fuel cell technology, and much effort is dedicated to finding anode catalysts with improved CO tolerance.[1−7] In the case of the electrooxidation of hydrogen-rich gases (H_2/CO mixtures), the removal of adsorbed CO is the rate-determining step over the entire potential range where significant amounts of absorbed CO exist. Similarly, in case of methanol electrooxidation, the removal of adsorbed CO, formed by methanol adsorption, is the rate-determining step at potentials below 0.5 V/RHE;[2,5] at higher potentials, the adsorption of methanol begins to govern the overall rate, with formate emerging as an additional reactive intermediate.[5] As a result of this, at low temperatures, the Pt 90 Ru 10 alloy surface, which supports a higher rate of methanol adsorption due to an "ensemble effect",[2] shows a higher methanol oxidation rate than the Pt 50 Ru 50 surface.

In the present paper, we discuss and compare an efficient experimental and theoretical−computational search strategy to predict and develop three- and four-component (ternary, quaternary) fuel cell alloy catalysts that are more active and more resistant against CO surface poisoning than the PtRu system. The two strategies include combinatorial and high throughput electrocatalytic experimentation on one hand and theoretical density functional theory (DFT) calculations in combination with

* Corresponding author. E-mail: pstrasser@symyx.com.

10.1021/jp030508z CCC: $25.00
Published on Web 09/17/2003

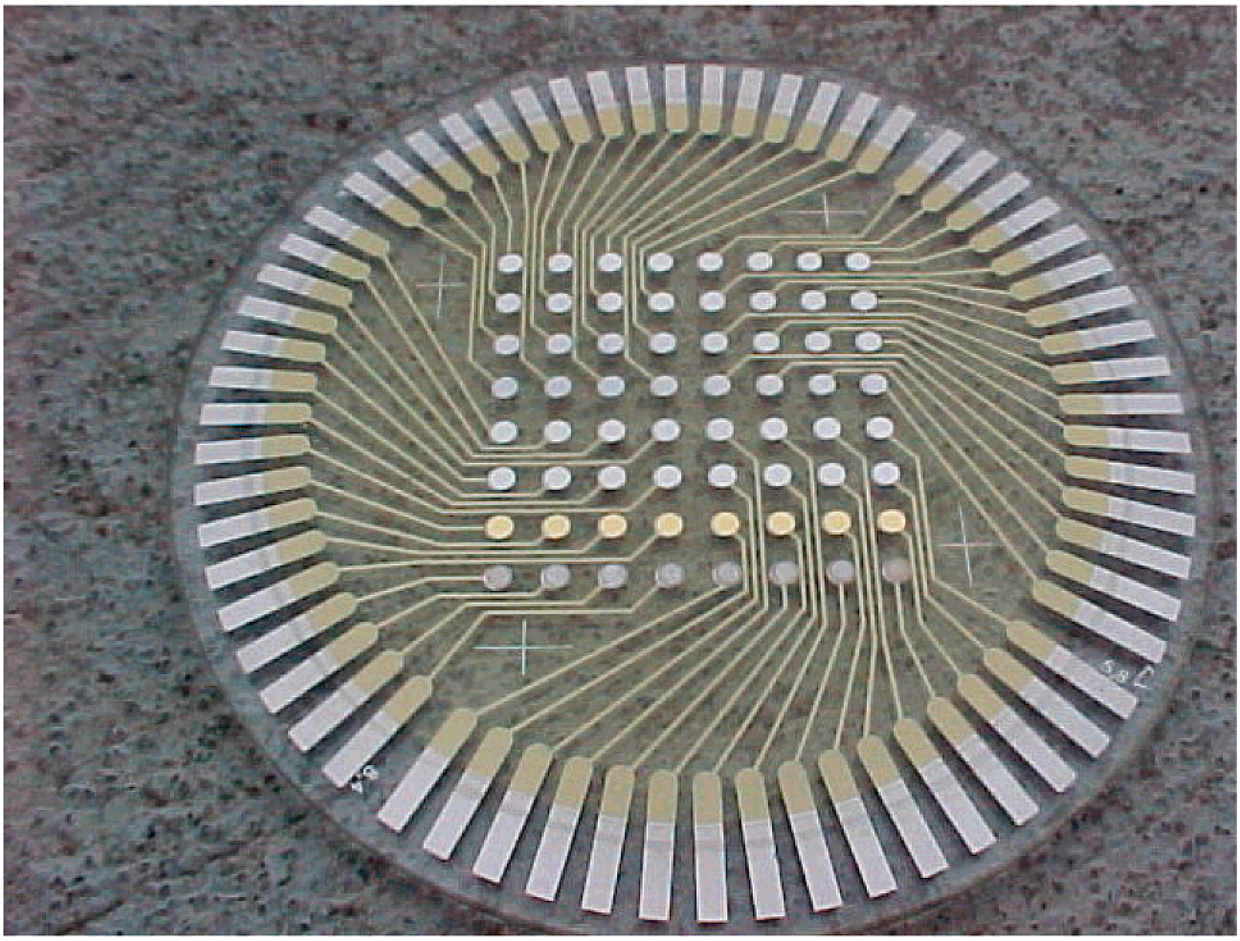

Figure 1. A 64-element addressable electrode array on a 3″ quartz wafer is used as support for the synthesis of chemically diverse electrocatalyst libraries.

micro kinetic modeling on the other. While these two methods vary vastly in their assumptions, strengths, and limitations, upon combination they represent a powerful and efficient tool for the exploration of new catalysts. We have used these two very different approaches to generate an activity map of a large portion of the anode materials landscape in a search for improved fuel cell anode catalysts; we show that the two independent searches point toward very similar ternary and quaternary Pt alloys with improved activity.

Combinatorial chemistry and combinatorial material science have become the general terms for all experimental strategies and methodologies that aim at accelerating the speed of chemical experimentation and of collection of chemical information.[3,4,8−10] Combinatorial chemistry typically involves parallel synthesis, characterization, and high-throughput screening of diverse arrays of materials (associated into a materials library), thereby allowing the rapid exploration of high-dimensional parameter spaces compared to conventional one-by-one sample approaches. Generally, at the primary high-throughput screening level, a large number of diverse miniature materials samples are synthesized and screened in parallel. While this approach does not always allow for an experimental precision comparable to a larger-scale experiment, it is designed such that observed *trends* in the desired materials properties such as catalytic activity remain significant. A follow-up screen on a larger scale is typically necessary to confirm and optimize the initial material hits or to collect more precise kinetic data.

On the theoretical side, with the development of DFT, we now have at our disposal a theoretical method that can be used to describe chemical bonding in the complex systems needed to describe the surface of catalysts. The accuracy of the calculated adsorption energies and activation barriers is not good enough that absolute rates of chemical reactions can be calculated accurately, but again *trends* in the reactivity from one catalyst to the next can now be calculated with sufficient confidence.[11,12]

2. Experimental, Theoretical, and Computational Methods

2.1. Experimental Combinatorial and High-Throughput Electrocatalysis. Combinatorial catalyst synthesis and high-throughput electrochemical screening are achieved by a proprietary array of 64 individually addressable, circular electrode pads, fabricated using lithographic techniques on an insulating 3″ quartz wafer[13] (Figure 1). Each pad is approximately 1.7 mm in diameter (∼0.02 cm^2 area).[9,10] The electrode pads are providing ohmic contacts with the catalytic electrode materials to be deposited thereon, interfacing the materials library and a multichannel potentiostat/galvanostat (Arbin Instruments Inc.). The material of the 64 supporting electrodes was chosen to be Titanium, which is chemically inert and noncorrosive under the chosen experimental conditions.

For the rapid, parallel synthesis of the 64-element metal alloy electrocatalyst library, automated rf-magnetron vacuum sputtering was employed. The individual constituents of the synthesized catalyst composition were deposited onto the 64-element electrode array using contact masks (see Figure 2a).[9,10] A proprietary moving-shutter technique allowed the controlled deposition of thin-film gradients ranging from a few Angstroms

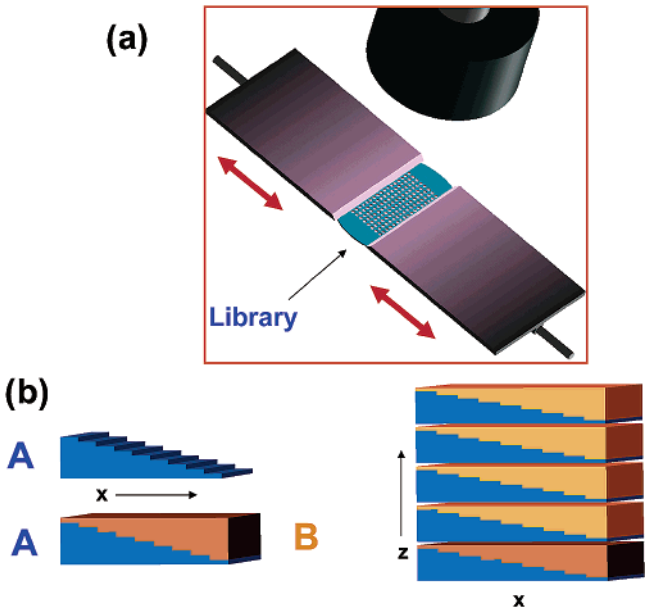

Figure 2. (a) An Rf magnetron sputter technique with automated target selection as well as automated moving shutters and physical shadow masking is employed for deposition of the electrocatalyst libraries. (b) Sequential gradient sputtering of very thin material slabs lead to in-situ thin-film alloy formation on the contact spots. The width of the slabs on the left extends over the entire width of the electrode array. Superlattice deposition in *z* direction results in the buildup of thicker films of the desired stoichiometric gradient.

to several micrometers.[13] Compositional variations in the thin-films were achieved either by sputtering parallel and orthogonal thickness gradients (see Figure 2b) or by sputtering multiple nongradient metal slabs of varying thickness. Typical individual gradient sputtering steps cover a thickness range of about 5−15 Å (Figure 2b, left). Sputtering of superlattice structures as shown on the right of Figure 2b eventually led to the buildup of thin-film thicknesses of up to several thousand Å. The deposition conditions were chosen such that the multi-element superlattice structures underwent in-situ atomic mixing of their individual materials components. X-ray diffraction studies confirmed complete and uniform alloying of the thin films.[13] Auger spectroscopic investigations of the alloy surfaces of sputtered, nonannealed thin films showed that the surface compositions were very close to the bulk composition. This observation was similar to results on sputter-cleaned, arc-melted bulk catalysts.[14]

For electrochemical characterizations, the array of electrocatalysts was combined with a cylindrical cell body such that all 64 electrocatalysts were facing upward and were exposed to the electrolyte. All contact pads at the edge of the wafer were isolated from the electrolyte using an O-ring seal. A Pt-mesh of about the same circular area as the cross section of the cylindrical cell body was placed in parallel to the quartz wafer at a distance of about 5 cm and served as the common counter electrode. A Hg/Hg_2SO_4 electrode was used as reference electrode. The electrode was sitting in a glass compartment with Luggin-Haber capillary, which was filled with base electrolyte. The capillary tip of the reference electrode compartment was placed between the working electrode array and the counter electrode mesh. The distances between the capillary tip of the reference compartment and the working electrodes at the edge and at the center of the array ranged from about 3 to 4 cm. This distance was chosen to be large compared to the distance between individual working electrodes (about 3 mm) to minimize differences in the uncompensated ohmic resistance between catalysts. Voltage drops across the electrolyte between the reference electrode tip and individual working electrodes were considered negligible given the conductivity of the electrolyte and the magnitude of the measured currents. The cell body was further equipped with gas inlet channels for purging the electrolyte with Argon, a gastight lid, and a conventional liquid-seal gas outlet. All potentials in this study will be referred to with respect to the reversible hydrogen scale (RHE) scale with an assumed potential difference of +0.65 V between the two scales.

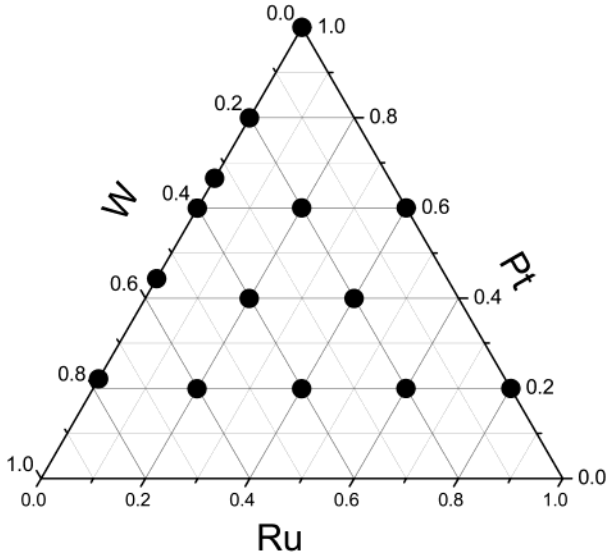

Figure 3. Example of a ternary metal alloy compositional space sampled and screened. Black dots indicate individual stoichiometries synthesized in the electrocatalyst library. Emphasis was placed on the six ternary stoichiometries Pt/A/B (20:20:60, 40:40:20, and all permutations thereof). The other five ternary systems were sampled accordingly.

The anode catalysts were electrochemically pretreated using repeated voltammetric cycling of all 64 catalysts between 0 and 0.7 V/RHE in 0.5 M H_2SO_4 at a rate of 20 mV/s and 200 mV/s. The pretreatment was stopped as soon as a time-stable voltammogram was obtained for most compositions. Some alloy compositions appeared to continue to change their base voltammetry, especially at large overpotentials, which is likely to indicate corrosive degradation and limited stability of those compositions; those same compositions also exhibit very large hydrogen adsorption integrals. The hydrogen adsorption charge of each catalyst over a potential range of 0.05−0.35 V/RHE on the slow voltammograms was used as an estimate of its active surface area using a hydrogen electrosorption pseudocapacity of 210 C/cm^2. Subsequently, the catalyst array was evaluated with respect to its methanol oxidation activity in a 1 M methanol, 0.5 M sulfuric acid electrolyte. Parallel linear potential scans and parallel chronoamperometric screening (+0.45 V/RHE, 5 min) of all catalysts yielded current density−time curves, as shown in Figure 4. All experiments were performed at ambient pressure and room temperature.

Pt, Ru, Co, Ni, and W were chosen as variables spanning the compositional space screened in this study, with Pt being a constituent in all catalysts (Pt-alloy catalyst concept). This combination of compositional space and constraints resulted in a total of six ternary systems (Pt plus RuCo, RuNi, RuW, CoNi, CoW, and NiW) to be screened. Figure 3 illustrates the typical degree of sampling of each ternary system. Six ternary compositions were synthesized for each ternary system, in particular, the three 20:20:60 and the three 40:40:20 compositions. The design also included a pure Pt catalyst, and a number of binary PtRu catalysts that were used as standard catalysts against which

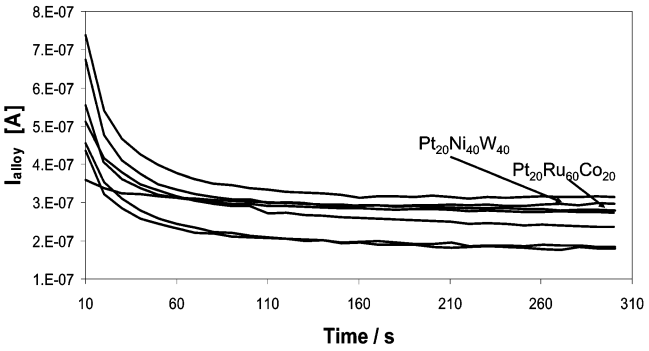

Figure 4. Parallel chronoamperometric screening of an electrocatalyst library. Shown are the measured current−time curves of the seven most active compositions after a potential step ($t = 10$ s) from open circuit potential (OCP) to +450 mV/RHE. During the inital 10-s period, the OCP was measured. Shown are channels 2,3,4,10,19,42,43; compare Figure 6a. Stoichiometric information is given for two active compositions. Conditions: 1 M Methanol, 0.5 M H_2SO_4, room temperature, $E = +450$ mV/RHE.

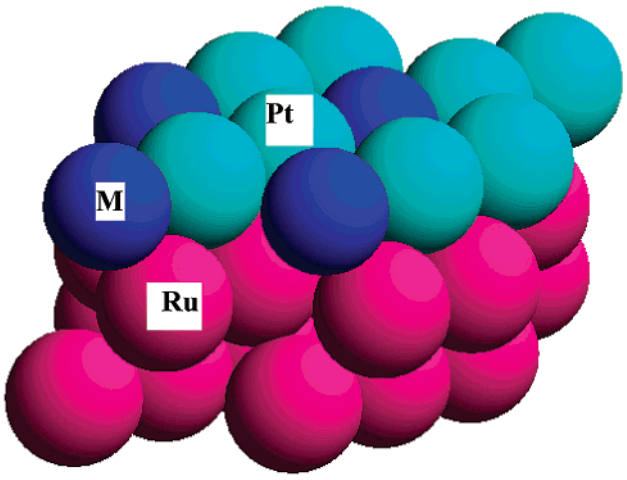

Figure 5. Schematic structures of ternary alloy on Ru(0001) surface, MPt_2/Ru, with M being one metal from the set {Fe,Co,Rh,Ir,Ni,Pd,-Pt,Cu,Ag,Au,Sn}. Metal M, dark blue ball, is the third kind of metal alloyed on the surface; Pt, green ball, is the fixed composition on the surface in this case. Ru, red ball, is the substrate (bottom two layers).

the activites of higher-order alloys were evaluated.[15] A repeat sample of the Pt:Ru 6:4 catalyst provided a measure of the experimental error of the experimental method.

2.2. Theoretical And Computational Screening of Anode Electrocatalysts. *Calculation Method*. In the present calculations, the Kohn−Sham one-electron valence states are expanded in a basis of plane waves with kinetic energies below 25 Ry, and ultra soft pseudopotentials are used to describe the ion cores.[16] The exchange−correlation energy and potential are described by the generalized gradient approximation (PW91).[17,18] The self-consistent electron density is determined by iterative diagonalization of Kohn−Sham Hamiltonian, Fermi population of the Kohn−Sham states at $k_BT = 0.1$ eV, and Pulay mixing of the resulting electronic density.[19]

In all cases, we use a three-layer slab with a $2\sqrt{3} \times 2\sqrt{3}$ (defined on the basis of all surface atoms being equivalent) surface unit cell as shown in Figure 5.

The two bottom layers are a Ru substrate. The surface layer includes Pt and another one or two kinds of metals as shown in Figure 5. Periodic boundary conditions are applied in the two directions parallel to the surface. In the calculation, the CO and H (dissociated H_2) adsorption energies at coverage of 1/12ML are considered for each system. In fact, higher CO coverage is relevant for electrode surfaces under electro-catalytic conditions. There are strong CO−CO repulsions at these coverages and the adsorption energy decreases strongly with increasing coverage. We are not including these effects here, because we are only interested in *relative* adsorption energies, that is, the change in adsorption energy from one surface to the next. This eliminates many systematic errors in the DFT calculations (e.g., coverage dependent adsorption energies as long as the adsorbate−adsorbate interactions are approximately the same on different surfaces). Atomic hydrogen is always adsorbed in the 3-fold hollow site on the surface. This is generally found to be the most stable site for hydrogen adsorption on close-packed surfaces.[20] Carbon monoxide is adsorbed in the atop site at low coverage. This is the site where CO is found experimentally to adsorb for all metals except Pd and Ni.[21] In each case, we consider adsorption on all possible metal atoms in the surface. In all cases except the Fe/Pt/Ru surface, CO prefers Pt at the surface (or to block Ru if available). In the calculations, all degrees of freedom of the CO and H are allowed to relax while the positions of all the metals in the systems are fixed at the lattice position of the substrate. We have checked that the fixed substrate does not affect relative adsorption energies of interest in the present work.

Kinetics. According to kinetic studies of the anode of a fuel cell,[22,23] the whole process is most simply described as a competition of CO and H_2 adsorption. The analysis indicates that the anode catalysts with better CO tolerance are the Pt alloys that bond CO more weakly than pure Pt, while still dissociating H_2. The competition between the ability of the surface to dissociate and bond hydrogen and not bond CO is conveniently described by the parameter[22,23] $-1/2\ \Delta E_{H_2} + \Delta E_{CO}$. ΔE_{H_2} is the adsorption energy of H_2, so half of that is the bond energy per H atom, while ΔE_{CO} is the adsorption energy of CO. Because we count the adsorption energies as negative for exothermic adsorption, a value of $-1/2\ \Delta E_{H_2} + \Delta E_{CO}$, which is larger than the value for pure Pt, means that CO adsorption is losing out to H adsorption and the surface should be more CO tolerant than Pt. To set the scale of the effects, we note that an increase in ΔE_{CO} by 0.1 eV (10 kJ/mol) for a fixed H_2 adsorption energy will lead to a decrease in the anode voltage drop about the same order of magnitude in the presence of 250 ppm CO at 60 °C.

In the following, we calculate $-1/2\ \Delta E_{H_2} + \Delta E_{CO}$ for all the systems we consider and use that as our measure of the CO tolerance.

3. Results

3.1. Combinatorial and High-Throughput Experimental Catalyst Screening. The electrocatalytic activity of the 64-element PtRuWCoNi library was evaluated in high-throughput screening mode using anodic potential sweep and chronoamperometric potential step methods. Figure 4 shows a chronoamperometric measurement of all 64 catalysts at +450 mV/RHE over 5 min. While the methanol oxidation currents of most catalysts remained below absolute currents of 0.1 μA (0.005 mA/cm^2 geometric current density), a few compositions exhibited very high sustained activity. The chronoamperometric profiles of all catalysts follow the familiar pattern of rapidly decaying capacitive current contributions followed by a slow asymptotic approach of a stationary-state activity. Figure 6a and Figure 6b report the final geometric current densities $J = I_{alloy}/A_{geometric}$ after 5 min of each individual channel over their channel numbers. The high-activity channels are labeled with their chemical compositions. The pure Pt standard catalyst was

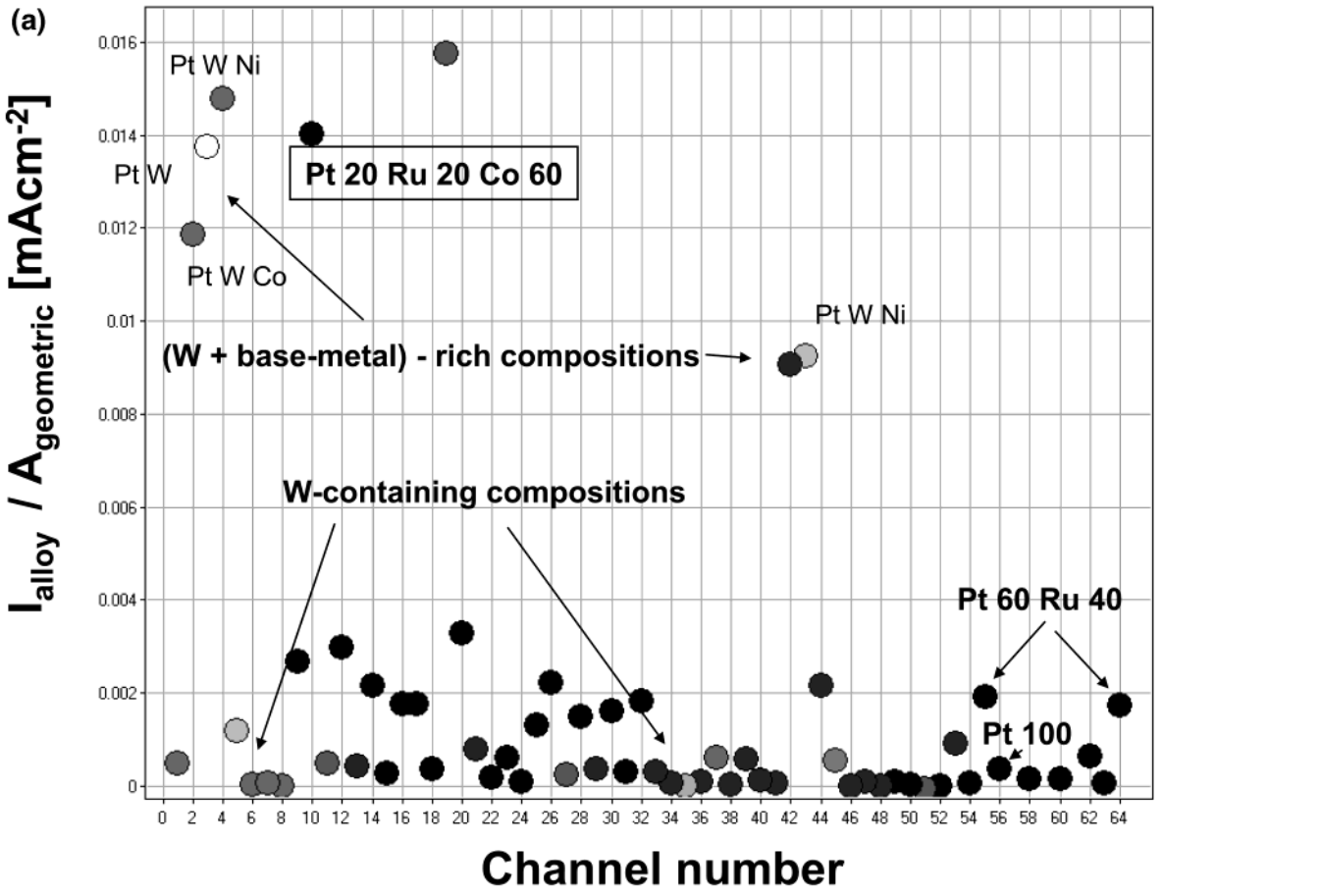
(a)
Pt W Ni
Pt W
Pt W Co
Pt 20 Ru 20 Co 60
(W + base-metal) - rich compositions
Pt W Ni
W-containing compositions
Pt 60 Ru 40
Pt 100
I_{alloy} / $A_{geometric}$ [mAcm^{-2}]
Channel number

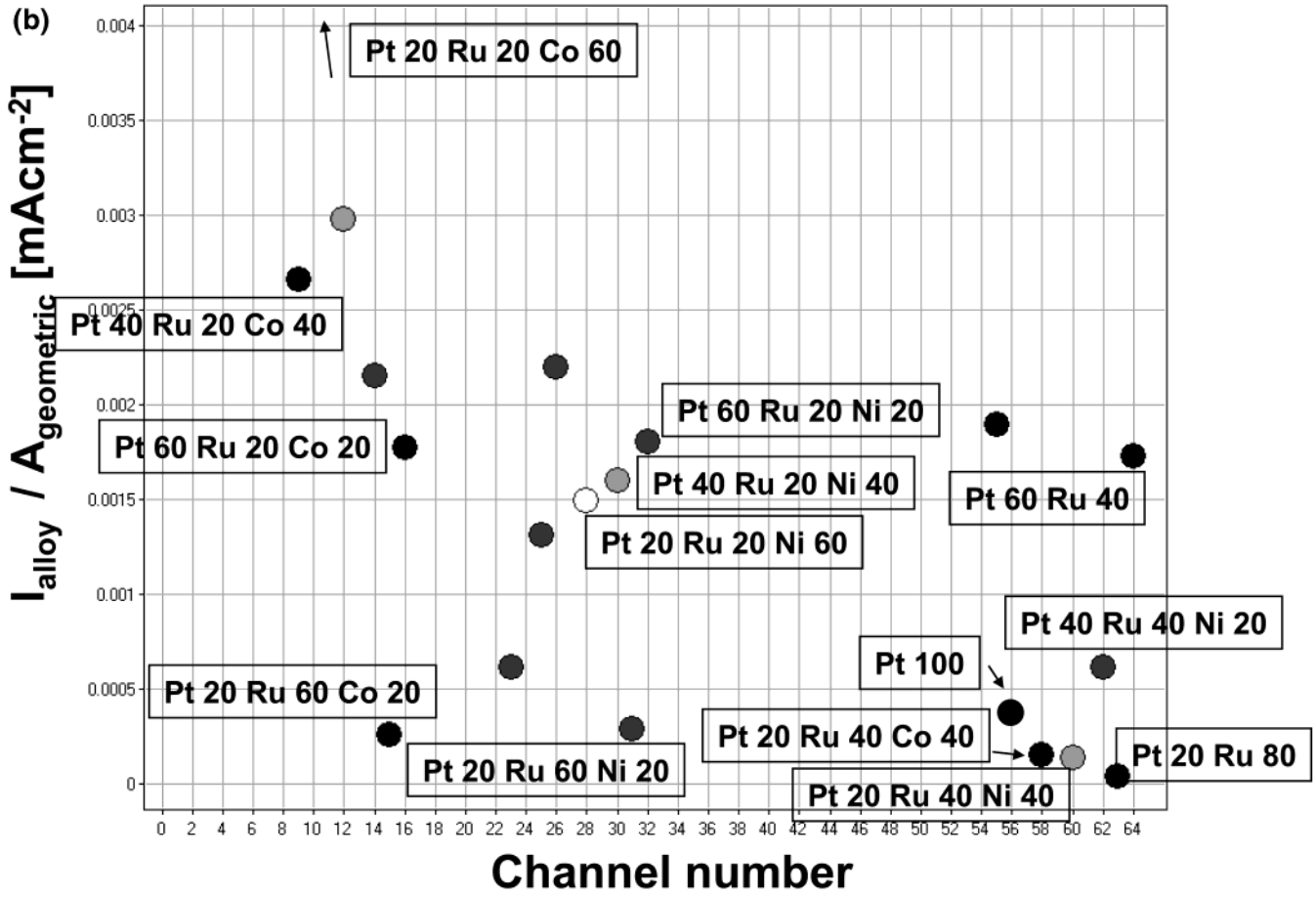
(b)
Pt 20 Ru 20 Co 60
Pt 40 Ru 20 Co 40
Pt 60 Ru 20 Co 20
Pt 60 Ru 20 Ni 20
Pt 40 Ru 20 Ni 40
Pt 20 Ru 20 Ni 60
Pt 60 Ru 40
Pt 40 Ru 40 Ni 20
Pt 100
Pt 20 Ru 60 Co 20
Pt 20 Ru 40 Co 40
Pt 20 Ru 80
Pt 20 Ru 60 Ni 20
Pt 20 Ru 40 Ni 40
I_{alloy} / $A_{geometric}$ [mAcm^{-2}]
Channel number

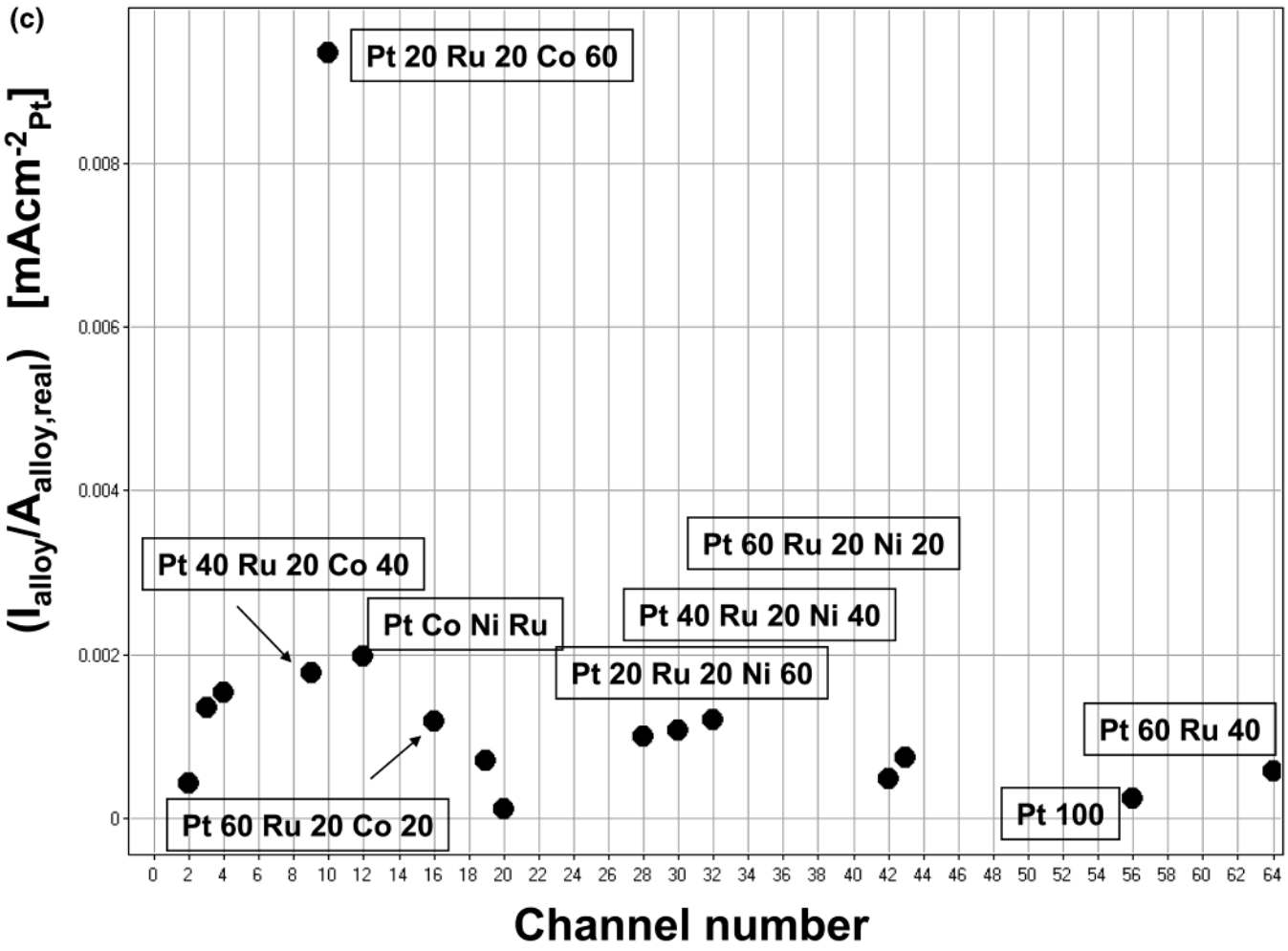

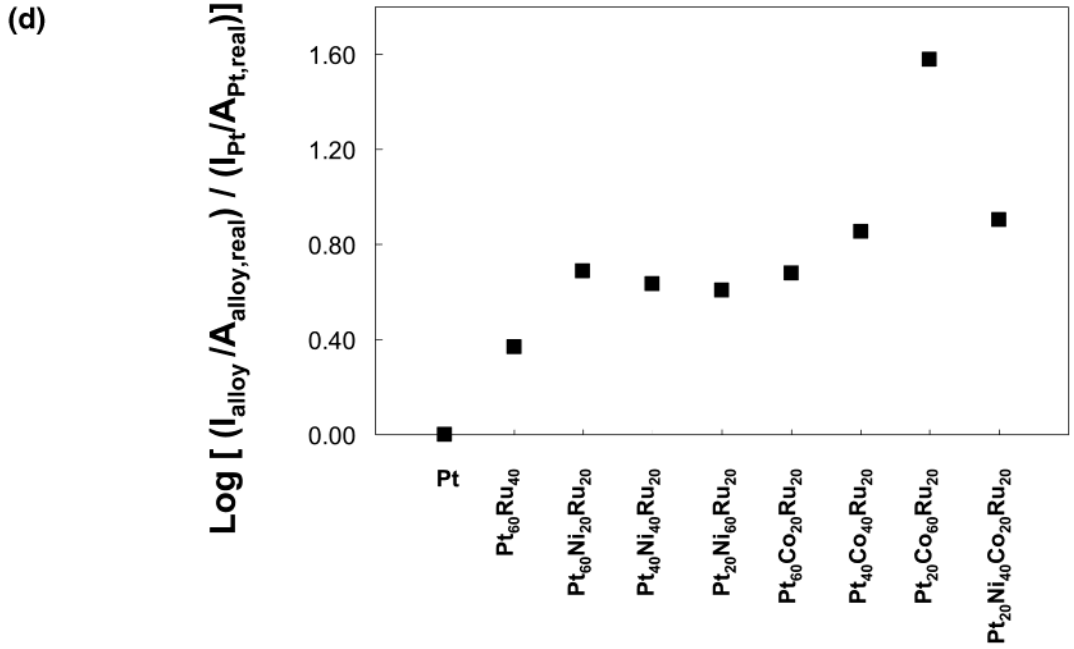

Figure 6. (a) Screening results of the chronoamperometric screen in Figure 4. Dots indicate the final chronoamperometric geometric current density of each channel. The gray coloring of the dots encode the W content of the electrocatalysts (white = high, black = low). The composition of a few active channels are indicated (b). Blow-up of the low-activity portion of (a) with all W-containing alloy catalysts removed. Indicated are the ternary alloy catalysts of interest. PtRu binary as well as the pure Pt spot serve as standards. Gray-coding indicates Ni content of the catalysts (white = high, black = low). (c) Pt surface-area normalized electrochemical activity (area-specific activity) of the most active alloys. The Pt surface-area was determined electrochemically using the hydrogen adsorption integral of each individual catalyst. (d) Summary of *activity trends* in (c). Plotted are the area-specific activities of (c) after normalization with repect to pure Pt. The logarithmic value represents an activation energy difference (relative kinetic improvement) and follows the DFT-calculations. Obvious are the gains in activity going from pure Pt, to PtRu, PtRuNi, and PtRuCo compositions. Quaternary compositions offer additional potential for improvements.

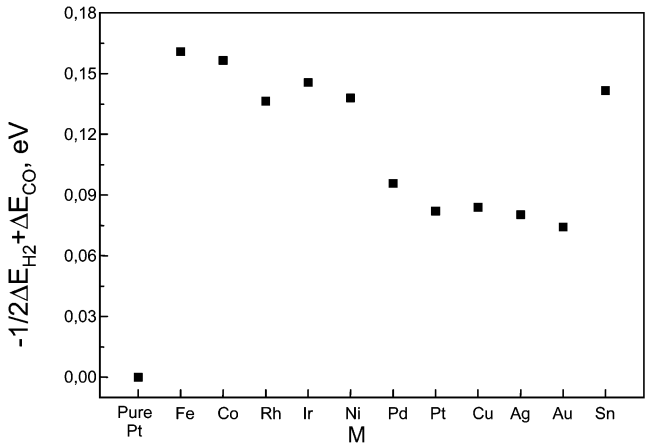

Figure 7. The surface activities of various ternary alloys, MPt_2/Ru. The alloyed atom on the surface, M, are respectively listed along the horizontal axis: "Pure Pt" = monometal Pt; Pt = binary alloy Pt/Ru. The corresponding atomic structure is shown in Figure 5. The surface contains 2/3ML Pt and 1/3ML "M". The observed activity trend from Pt to PtRu to PtRuNi to PtRuCo is similar to the trends observed in the experimental screening experiments.

deposited on channel 56. The observed geometric current density observed for the Pt standard catalyst compares well with those reported on sputter-cleaned smooth alloy catalysts: At +450 mV/ RHE, the pure Pt catalyst exhibited an initial geometric current density of about 2.5 μA/cm^2, which dropped to 0.5 μA/cm^2 after 5 min. In comparison, in Figure 7c of ref 14, a study performed in 0.5 M methanol, a sputter-cleaned Pt electrode showed an initial geometric current density of about 3 μA/cm^2.

As commonly known, alloying Pt with Ru increases the catalytic activity strongly[1,2,14] The variation between the two Pt/Ru 6:4 spots (channels 55 and 64) yields a rough measure of the experimental error of the screening method; from that, it is obvious that some of the 64 catalysts show large, statistically significant activity improvements over the PtRu compositions. As an additional cross-check of the high-throughput method, channel 63 (Figure 6b) reports the activity of a Ru-rich PtRu alloy catalyst (Pt/Ru 20:80). As expected, high Ru contents are detrimental to the methanol oxidation activity leading to activities lower than Pt itself.

On the basis of the data in Figure 6a, the following composition-activity relationships within the 64 electrocatalysts can be identified: First, most W-containing, gray-shaded compositions show very low to no current activity (marked as "W-containing" in Figure 6a). A closer look at the compositions of these catalysts reveals that their combined molar fractions of all three base metals ($x_W + x_{Co} + x_{Ni}$) roughly equals 0.5−0.6. Second, there is a group of very active W-containing, Ru-free compositions with a combined base-metal molar fraction ($x_W + x_{Co} + x_{Ni}$) of about 0.8. Due to their high base metal content, these compositions undergo strong surface corrosion and surface roughening during the pretreatment leading to high current densities due to their increased surface area; this is confirmed by their much larger H-adsorption integrals in base electrolyte compared to the Pt or PtRu catalysts. Finally, there is a group of W-free electrocatalysts (black dots in Figure 6a, labeled compositions in Figure 6b) that are, with one exception, clustered closer around the PtRu reference activity. Among them, Ru-rich compositions exhibit a lower activity than the PtRu standards (see Pt 20 Ru 60 M 20 and Pt 20 Ru 40 M 40 with M = Co,Ni, channels 15,31,58,60). For PtRuNi, as the Pt content is increased at constant Ru, the activity rises to levels comparable to the PtRu standard (channel 28,30,32).[24] In the case of PtRuCo, however, the Co-rich Pt/Ru/Co = 1:1:3 exhibits very high activity (channel 10, $Pt_{20}Co_{60}Ru_{20}$), and as Pt replaces Co (channels 9,16) the activity drops stepwise to levels comparable to PtRu.

To rank and prioritize alloy electrocatalyst with respect to their intrinsic catalytic activity, electrochemical current data is typically normalized to the real surface area of the catalysts rather than to their geometric surface area. Figure 6c reports the Pt-area-normalized electrochemical activity of the most active alloy catalyst compositions. These activities were obtained dividing the absolute measured currents I_{alloy} of each catalyst by its real Pt surface area as determined electrochemically using the respective hydrogen adsorption integral. The order of activity of the most active electrocatalysts has obviously changed based on their electrochemically determined Pt surface area. In particular, analysis of the real surface area of Pt/Ru/Co 20:20:60 (channel 10) reveals no significant increase of its true surface area by corrosion compared to the PtRu standards, which indicates a favorable degree of stability and gives rise to a significant intrinsic activity improvement for this compositions. This is in contrast to the active W-containing compositions that appear to corrode more severely and show reduced specific activity after correction for their surface area; while a few W-containing catalysts still maintain activities comparable or slightly better than the standards, their longer-term stability remains questionable.

Figure 6d summarizes the basic trends of this experimental study that are to be compared to the theoretical screening results: The Pt-area-normalized activities of some active PtNiRu and PtCoRu compositions were normalized to that of pure Pt and plotted on a logarithmic scale. The physical meaning of the quantity plotted on the *y* axis would correspond to a Butler−Volmer exponent, which is a potential-dependent activation energy difference and follows the theoretical computer figure (see next paragraph). Figure 6d highlights the catalytic activity gains of ternary alloys starting from pure Pt followed by PtRu, PtRuNi, and PtRuCo compositions.[24] Furthermore, quaternary alloy compositions, although not systematically studied here, are shown to offer additional potential for catalyst improvements or cost reduction.

3.2. Theoretical and Computational Catalyst Screening. The theoretical screening results of a number of PtRuM (M = transition metal shown along *x*-axis) ternary alloys are shown in Figure 7. Clearly, all the ternary as well as the PtRu bimetallic alloy (M = Pt) are superior to pure Pt as anode catalysts. In particular, M = Fe, Co, Rh, Ir, and Sn/Pt/Ru show much better CO tolerance and therefore catalytic activity than Pt or PtRu. While not as active as Fe or Co, PtRu−Ni also showed considerable improvements in CO tolerance compared to PtRu. Figure 8 reports the CO-tolerance (activity) versus alloy stoichiometry. Surface content of the alloyed metal, M, between 1/3 and 2/3 displayed the best performance.Finally, computational results in Figure 9 indicate that quaternary alloy catalysts consisting of Co, Fe, Pt, and Ru appear to be even slightly more active than the ternary electrocatalysts.

4. Discussion

Experimental and theoretical high-throughput strategies for rapid screening of new materials have been described and studied comparatively. Both methods were applied for the predictive and experimental screening of highly active, ternary PtRu−X alloy anode fuel cell catalysts, and their results were compared. Independently, both methods revealed similar activity *trends* of the PtRuX alloys, as the third metal X is varied among

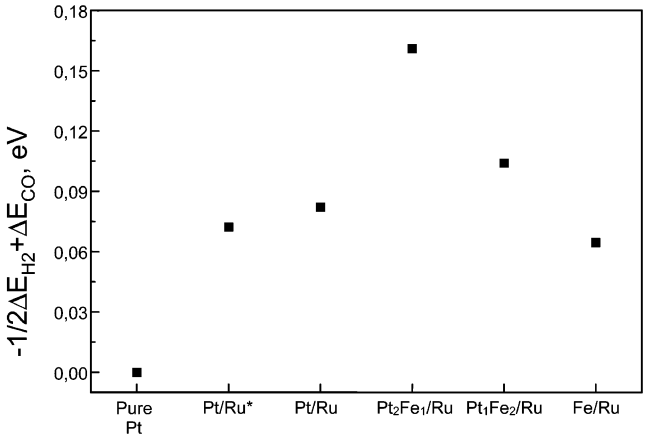

Figure 8. The surface activities of Pt_xFe_y/Ru (x,y=0,1/3,2/3,1) with different Fe and Pt content. Pure Pt = monometal Pt. Pt/Ru indicates a Pt monolayer slab on top of two Ru slabs as given in Figure 7, while Pt/Ru* indicates a Pt2Ru surface alloy slab on top of two Ru slabs.

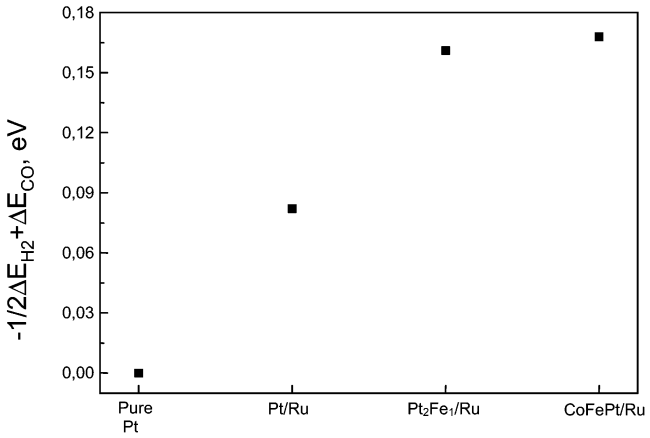

Figure 9. The surface activities of quaternary alloy CoFePt/Ru. Pure Pt = monometal Pt. The surface contains 1/3ML Pt, 1/3ML Fe, and 1/3ML Co.

the transition metals. In addition, activity trends from both methods within a given ternary system appear to point to similar optimized ratios of the molar fractions of the alloy metals.

The experimental thin-film screening aimed at identifying ternary metal alloys PtRuM for methanol electrooxidation, where M = Ni,Co,W, with higher electrochemical activity compared to Pt and PtRu standard catalysts. High-throughput screening methods rely on simplifications of the realistic materials environment by eliminating parameters that are not considered significant for the improvement of the materials properties. In the present case of anode fuel cell catalysts, the influence of the supporting carbon of the conductive polymer and other parameters associated with a gas-diffusion electrode were neglected by using a sputter-thin-film approach. Sputtered thin-films, unlike alloy electro-co-deposition methods, allow a more precise control of the alloy stoichiometry, and are typically dense and very smooth so that the initial real electrode surface area of each catalyst is essentially equal to the geometric area of the supporting electrode pad. This facilitates a direct comparison of catalytic activities of different alloys based on geometric current activity only, provided a similar Pt molar fraction and no significant change of the surface area by, for instance, corrosion. Still, for alloys that are not corrosion-stable, quantifying of and correction for the extent of surface area change over time is crucial for a fair comparison of the specific activities of electrocatalysts. Within the PtRu−Co−Ni ternary compositional space, PtRuCo ternary catalysts clearly outperformed the PtRu standard catalyst, followed by PtRuNi ternary catalyst; this order of activity agrees favorably with a recent study of ternary methanol electrocatalysts electrodeposited onto organic polymer films where PtRuCo outperformed PtRuNi followed by PtRu catalysts.[6,25] In the present study, the best performing Co-containing ternary catalyst at channel 10 ($Pt_{20}Co_{60}Ru_{20}$) contained a nominal Pt/Co ratio of 1:3; following ref 14, its Co surface content can be estimated to be around 3/5, assuming no significant surface segregation within sputtered thin-films.

The mechanism of the experimental activity enhancement remains speculative, but could be rationalized as follows: At potentials below 0.5 V/RHE, the methanol oxidation on PtRu binary alloys is rate limited by the availability of free surface sites for methanol adsorption and dehydrogenation.[2] The number of free surface sites can be increased by an enhanced oxidative removal of adsorbed CO by oxygenated species adsorbed on the base metal component (*enhanced bifunctional effect* of a ternary alloy) or else by decreasing the CO coverage of the surface by changing the CO adsorption energy (*ligand effect* of a ternary alloy). The ligand effect would make the formation of the adsorbed intermediate CO less favorable, while the formation of a reactive intermediate could be preferred. While both mechanisms rely on the availability of oxygenated species (adsorbed water or OH) in the neighborhood of methanol adsorption sites and, in this sense, are bifunctional, the ligand effect explicitly relies on the combined presence of Ru and Co in the right stoichiometric ratio. In fact, neither Pt 20 Ru 80 nor Pt 20 Co 80 shows a methanol oxidation activity similar to Pt 20 Co 60 Ru 20.

The observed activity of Pt/Ru/Co 1:1:3 is almost eight times as high as the PtRu standard catalysts and about 37 times higher than the Pt standard catalyst. These observed large activity increases raise the question as to the quantitative predictive power of the experimental screening method. High throughput screening methods of thin-film electrocatalysts, just like any other primary high throughput screening method, effectively detect *trends* in the materials property of interest such as the intrinsic electrocatalytic activity as a function of composition. While the trends in catalyst activity typically remain valid after proper scale-up, large geometric or specific activity enhancements of thin-film electrocatalysts may vary upon scale-up, especially if a different catalyst format (e.g., a supported particle catalyst) is employed. This has been observed in a number of earlier studies of thin-film and corresponding powder electrocatalysts.[10,26−29] The variations in the enhancement factor may be due to one or more aspects such as differences in synthesis, differences in the active crystallographic phase, particle size effects,[26] differences in surface corrosion, or uniformity of alloying. Despite all these potential complications of varying catalyst formats, however, comparative studies of binary methanol oxidation and binary oxygen reduction catalysts have given evidence that *activity trends* of bulk or thin-film alloy systems qualitatively correlate with scaled-up powder catalysts and can help point to improved catalyst systems.[2,10,27,28,29]

The theoretical screening methods revealed a trend in the activity of ternary PtRuM (M from the set of transition metals in Figure 7) anode fuel cell catalysts. As observed in experiment (Figure 6d), the theoretical methods also obtain a trend of PtRuCo outperforming PtRu and PtRuNi compositions (Figure 7). It is only surpassed by M = Fe containing ternary catalysts. A closer look at the stoichiometry activity relationship revealed that for the most active transition metals, a surface content of M of 1/3−1/2 yielded the highest activities. This is in reasonable agreement with the experimental finding of an optimal Co

surface content of 3/5 (Pt/Ru/Co 1:1:3). Furthermore, quaternary alloy catalysts were found to offer additional potential for catalyst improvements.

As detailed in refs 22 and 23, the great advantage of the theoretical screening lies in its ability to help clarify the mechanistic origin of the promoting effect of alloying PtRu with additional metals based on the $-^1/_2\ \Delta E_{H_2} + \Delta E_{CO}$ value. The modeling suggests that the increase in CO tolerance of PtRuX ternary alloys is based on a reduced CO adsorption energy on Pt sites, resulting in a smaller CO coverage and a larger number of sites for the primary oxidative process such as hydrogen or methanol oxidation.

5. Comparative Conclusions on Experimental and Theoretical Screening

It is the objective of the present study to demonstrate the complementary nature, as well as the power, of the combination of experimental and theoretical screening methods for the discovery of novel functional materials. While combinatorial experimental materials development essentially amounts to rapid material synthesis followed by selection, theoretical and computational materials research builds on the synthesis of new materials by design. While the combinatorial experimental screening is typically used for establishing empirical activity−property relationships requiring only limited hypothesis-driven input, the theoretical screening of materials using a DFT-micro kinetic model approach is dependent on a number of detailed structural, electronic and mechanistic assumptions. Yet both methods require a careful choice of the basic materials concept and materials compositional space to be screened, which requires at least some knowledge about the nature of the problem.

Conversely, high-throughput experimentation can also be used for extending or corroborating an already existing theoretical framework, while computational screening can allow for a inexpensive serendipity-driven exploration of materials compositional spaces. Also, both methods are highly data-driven, and therefore rely on the creation of a diversity of chemical data from which conclusions can be drawn.

As demonstrated in the case of fuel cell catalysts, the theoretical screening approach yields trends in detailed kinetic and thermodynamic parameters such as adsorption energies or activation barriers that are typically unavailable or inaccessible in experimental high-throughput screenings. The high throughput experiments, in contrast, yield trends in desired materials properties under *relevant* experimental conditions, as illustrated by the corrosion behavior of the alloy catalysts considered in Figure 6.

Even though the combination of both search strategies has become a powerful standard tool in pharmaceutical drug research, it is not as well established in other areas of research and development such as catalysis, electronic materials, or polymers. The present results should encourage the application of the described methods as a modern approach toward the development of novel functional materials.

References and Notes

(1) Lipkowski, J., Ross, P. N. *Electrocatalysis;* Wiley-VCH: New York, 1998

(2) Markovic, N. M.; Ross, P. N. *Surf. Sci. Rep.* **2002**, *45*, 117.

(3) Miertus, S.; Fassina, G. *Combinatorial Chemistry and Technology*, Marcel Dekker: New York, 1999. Xiang, X. Sun, X.; Briceno, G.; Lou, Y.; Wang, K.; Chang, H.; Wallace-Friedman, W.; Chen, S.; Schultz, P. *Science* **1995**, *268*, 1738. Jandeleit, B.; Schaefer, D. J.; Powers, T. S.; Turner, H.; Weinberg, W. H. *Angew. Chem. Int. Ed.* **1999**, *38*, 2495.

(4) Gurau, B.; Viswanathan, R.; Liu, R.; Lafrenz, T. J.; Ley, K. L.; Smotkin, E. S.; Sarangapani, S. *J. Phys. Chem. B* **1998**, *102*, 9997. Reddington, E.; Sapienza, A.; Gurau, B.; Viswanathan, R.; Sarangapani, S.; Smotkin, E. S.; Mallouk, T. E. *Science* **1998**, *280*, 1735.

(5) Chen, Y. X.; Miki, A.; Ye, S.; Sakai, H.; Osawa, M. *J. Am. Chem. Soc.* **2003**, *125*, 3680.

(6) Markovic, N. N.; Ross, P. N. *Electrochim. Acta* **2000**, *45*, 4101. Lamy, C.; Lima, A.; LeRHun, V.; Delime, F.; Coutanceau, C.; Leger, J.-M. *J. Power Sources* **2002**, *105*, 283.

(7) Park, K.-W.; Choi, J.-H.; Kwon, B.-K.; Lee, S.-A.; Sung, Y.-E.; Ha, H.-Y.; Hong, S.-A. Kim, H.; Wieckowski, A. *J. Phys. Chem B* **2002**, *106*, 1869.

(8) Nicolaou, K. C., Hanko, R., Hartwig, W. Handbook of Combinatorial Chemistry − Drugs, Catalysts, Materials; Wiley: New York, 2002.

(9) Strasser, P.; Gorer, S.; Devenney, M. *Proceedings of the International Symposium on Fuel Cells for Vehicles*, 41st Battery Symposium, The Electrochemical Society of Japan, Nagoya 2000, p 153. US Patent No.'s 6,187,164, 6,468,806, 5,985,356, and 6,004,617. Additional patents pending.

(10) Strasser, P.; Gorer, S.; Devenney, M. in *Direct Methanol Fuel Cells*, Narayanan, S. R., Gottefeld, S., Zawodzinski, T., Eds.; Proceedings Volume 2001−4, The Electrochemical Society: New Jersey, 2001, p 191

(11) Besenbacher, F.; Chrokendoff, I.; Clausen, B. S.; Hammer, B.; Molenbroek, A. M.; Nørskov, J. K.; Stensgaard, I. *Science* **1998**, *279*, 1913.

(12) Hammer, B.; Nørskov, J. K. in *Chemisorption and Reactivity on Supported Clusters and Thin Films*; Lambert, R. M., Pacchioni, G., Eds.; Kluwer Academic Publishers: The Netherlands, 1997.

(13) US Patent No.'s 6,045,671, 6,364,956, 5,985,356, 6,371,640 and 6,004,17. Additional patents pending.

(14) Gasteiger, H.; Markovic, N.; Ross, P. N.; Cairns, E. J. *J. Phys. Chem.* **1993**, *97*, 12020.

(15) It should be noted that the specific PtRu stoichiometry of 6:4 was not chosen deliberately, but rather resulted as a byproduct from the optimization of the library design in order to accommodate the desired 36 ternary compositions. The optimal Pt/Ru ratio for methanol oxidation is still not well established (see ref 6) even though Pt/Ru 1:1 is used most widely. Pt/Ru 1: 1 and Pt/Ru 6:4 were synthesized and tested side by side on separate material libraries where Pt/Ru 1:1 was found to be slightly more active. Because this study is interested in activity improvements of a much larger scale, the Pt/Ru ratio of 6:4 served as an acceptable alloy standard catalyst.

(16) Vanderbilt, D. *Phys. Rev. B* **1990**, *41*, 7892.

(17) Perdew, J. P.; Chevary, J. A.; Vosko, S. H.; Jackson, K. A.; Pederson, M. R.; Singh, P. J.; Fiolhais, C. *Phys. Rev. B* **1992**, *46*, 6671.

(18) White, J. A.; Bird, D. M. *Phys. Rev. B* **1994**, *50*, 4954.

(19) Kresse, G.; Furthmuller, J. *Comput. Mater. Sci.* **1996**, *6*, 15.

(20) Christman, K. *Surf. Sci. Rep.* **1988**, *9*, 1.

(21) Feibelman, P. J.; Hammer, B.; Nørskov, J. K.; Wagner, F.; Scheffler, M.; Stumpf, R.; Watwe, R.; Dumesic, J. *J. Phys. Chem. B* **2001**, *105*, 4018.

(22) Christoffersen, E.; Liu, P.; Ruban, A.; Skriver, H. L.; Nørskov, J. K. *J. Catal.* **2001**, *199*, 123; Liu, P.; Nørskov, J. K. *Fuel Cells* **2001**, *1*, 192.

(23) Liu, P.; Logadóttir, Á.; Nørskov, J. K. Modeling the electro-oxidation of CO and H_2/CO on Pt, Ru, PtRu and Pt_3Sn. *Electrochim. Acta*, accepted for publication.

(24) US Patent No. 6,517,965. Additional patents pending. US Patent application No. 2002/0146614, pending

(25) Lima, A.; Coutanceau, C.; Leger, J.-M.; Lamy, C. *J. Appl. Electrochem.* **2001**, *31*, 379.

(26) Min, M.; Cho, J.; Cho, K.; Kim, H. *Electrochim. Acta* **2000**, *45*, 4211.

(27) Toda, T.; Igarashi, H.; Uchida, H.; Watanabe, H. M. *J. Electrochem. Soc.* **1999**, *146*, 3750.

(28) Ralph, T. R.; Hogarth, M. P. *Platinum Metals Rev.* **2002**, *46*, 3.

(29) Mukerjee, S.; Srinivasan, S. *J. Electroanal. Chem.* **1993**, *357*, 201.